Development 136, 2335-2344 (2009) doi:10.1242/dev.031609

Sns and Kirre, the *Drosophila* orthologs of Nephrin and Neph1, direct adhesion, fusion and formation of a slit diaphragm-like structure in insect nephrocytes

Shufei Zhuang[1,*], Huanjie Shao[1,*], Fengli Guo[1], Rhonda Trimble[1], Elspeth Pearce[1] and Susan M. Abmayr[1,2,†]

The Immunoglobulin superfamily (IgSF) proteins Neph1 and Nephrin are co-expressed within podocytes in the kidney glomerulus, where they localize to the slit diaphragm (SD) and contribute to filtration between blood and urine. Herein, we demonstrate that their *Drosophila* orthologs Kirre (Duf) and Sns are co-expressed within binucleate garland cell nephrocytes (GCNs) that contribute to detoxification of the insect hemolymph by uptake of molecules through an SD-like nephrocyte diaphragm (ND) into labyrinthine channels that are active sites of endocytosis. The functions of Kirre and Sns in the embryonic musculature, to mediate adhesion and fusion between myoblasts to form multinucleate muscle fibers, have been conserved in the GCNs, where they contribute to adhesion of GCNs in the 'garland' and to their fusion into binucleate cells. Sns and Kirre proteins localize to the ND at the entry point into the labyrinthine channels and, like their vertebrate counterparts, are essential for its formation. Knockdown of Kirre or Sns drastically reduces the number of NDs at the cell surface. These defects are associated with a decrease in uptake of large proteins, suggesting that the ND distinguishes molecules of different sizes and controls access to the channels. Moreover, mutations in the Sns fibronectin-binding or immunoglobulin domains lead to morphologically abnormal NDs and to reduced passage of proteins into the labyrinthine channels for uptake by endocytosis, suggesting a crucial and direct role for Sns in ND formation and function. These data reveal significant similarities between the insect ND and the SD in mammalian podocytes at the level of structure and function.

KEY WORDS: Sns, Kirre (Duf), Nephrocytes, Slit diaphragm, Garland cell, Fusion

INTRODUCTION

In *Drosophila*, the Immunoglobulin superfamily (IgSF) proteins encoded by *kin of irre* [*kirre*; also known as *dumbfounded* (*duf*)], *roughest* (*rst*), *sticks and stones* (*sns*) and *hibris* (*hbs*) function as ligand-receptor pairs on the surface of founder cells and fusion competent myoblasts (Artero et al., 2001; Bour et al., 2000; Dworak et al., 2001; Ruiz-Gomez et al., 2000; Shelton et al., 2009; Strunkelnberg et al., 2001). These proteins mediate recognition, adhesion and fusion to form multinucleate syncitia through direct interaction at sites of myoblast contact. However, neither their action nor their expression is exclusive to the musculature, and previous studies noted their role in cell recognition and adhesion in the *Drosophila* eye (Bao and Cagan, 2005). Moreover, multiple studies have confirmed the presence of the *kirre* transcript and *sns* transcript in the binucleate garland cell nephrocytes (GCNs) (Duan et al., 2001; Ruiz-Gomez et al., 2000). These nephrocytes possess a structure visible by transmission electron microscopy (TEM) (Koenig and Ikeda, 1990; Kosaka and Ikeda, 1983) reminiscent of the slit diaphragm (SD) in the vertebrate kidney, and process waste products from the hemolymph (Aggarwal and King, 1967; Crossley, 1985). It is therefore compelling that the fly detoxification machinery may have similarities to that in mammals, and that Sns and Kirre play roles similar to those of their vertebrate counterparts.

Removal of waste products from the closed circulatory system of vertebrates takes place in the kidney glomerulus. Podocytes, kidney epithelial cells that surround the capillary blood vessels, extend foot processes that contact the surface of these vessels. Filtration then occurs as molecules flow out of the bloodstream through slits between adjacent foot processes into the urine (Barletta et al., 2003; Liu et al., 2003). Neph1 (Sellin et al., 2003) and Nephrin (Kestila et al., 1998), vertebrate orthologs of the above *Drosophila* IgSF proteins, localize to this filter (Holzman et al., 1999; Liu et al., 2003; Ruotsalainen et al., 1999) and appear to be an important determinant of glomerular permeability (Hamano et al., 2002; Liu et al., 2003). Mutations in *nephrin* and *neph1* are associated with congenital nephrotic syndrome as a consequence of defects in this filtration diaphragm. Lack of either *nephrin* or *neph1* leads to podocyte foot process effacement and detachment of podocytes from the glomerular basement membrane, loss of SDs, and proteinuria (Donoviel et al., 2001; Putaala et al., 2001).

In addition to their high degree of homology, Nephrin and Neph1 have other features in common with Sns and Kirre. Heterophilic interactions occur in trans between the extracellular domains of Nephrin and Neph1, and Sns and Kirre (Barletta et al., 2003; Galletta et al., 2004; Gerke et al., 2003). Studies have suggested that, in addition to serving as a scaffold onto which other proteins in the SD assemble, Nephrin and Neph1 function as signaling molecules to direct downstream cytoplasmic events (Benzing, 2004). They cooperate to transduce a signal that directs actin polymerization (Garg et al., 2007), and activation of this pathway occurs through interaction of phosphorylated tyrosines in the cytoplasmic domains of Nephrin and Neph1 to adaptor proteins (Jones et al., 2006; Verma et al., 2006). These adaptor proteins recruit components of the actin polymerization machinery that include N-WASp and Arp2/3 (Lu et al., 1997; Rohatgi et al., 2001). Similar phosphotyrosine modifications are important for Sns function (Kocherlakota et al.,

[1]Stowers Institute for Medical Research, Kansas City, MO 64110, USA. [2]Department of Anatomy and Cell Biology, University of Kansas Medical Center, MS3038, Kansas City, KS 66160, USA.

*These authors contributed equally to this work
†Author for correspondence (e-mail: sma@stowers.org)

Accepted 22 April 2009

2008) and studies have shown that the WASp and Arp2/3 actin polymerization machinery functions in *Drosophila* myoblast fusion (Berger et al., 2008; Kim et al., 2007; Richardson et al., 2007), probably downstream of Sns and Kirre.

The pericardial cells and garland cells comprise two subpopulations of *Drosophila* nephrocytes that, along with Malpighian tubules, form the excretory system (Crossley, 1985). Approximately 25-30 tightly associated binucleate GCNs encircle the anterior end of the proventriculus in a 'garland' at its junction with the esophagus (Aggarwal and King, 1967). The cortical region of the cytoplasm includes elaborate channels that are generated by invagination of the plasma membrane during embryogenesis and early larval instar stages. The initial invagination is associated with formation of a junction between two sites on the plasma membrane that are visible by TEM (Narita et al., 1989). Through a mechanism that is not entirely clear, this initial invagination expands into an extensive array of labyrinthine channels by the third-instar larval stage. The GCNs are very active in endocytosis via coated vesicles at sites deep within these labyrinthine channels (Wigglesworth, 1972). Thus, molecules to be eliminated must gain access to the endocytic machinery deep in these channels. These studies also identified a thin bridge spanning the channel opening that is visually similar to the vertebrate SD. The presence of Sns and Kirre and a slit diaphragm-like structure in these binucleate cells raised the possibility that these IgSF proteins might function in GCN fusion and/or in formation of this structure.

We demonstrate herein, as reported recently by others (Weavers et al., 2009), that Sns and Kirre are present in, and crucial for, the nephrocyte diaphragm (ND). Knockdown of Kirre or Sns results in a severely diminished number of NDs and smoothening of ND-associated furrows on the GCN surface, implicating Sns and Kirre in their formation. Mutations in the extracellular domain of Sns cause major perturbations in the ND, establishing that Sns also dictates fundamental aspects of its structure. Similar smoothening of the GCN surface occurs upon knockdown of Polychaetoid (Pyd) (Chen et al., 1996; Takahisa et al., 1996), the *Drosophila* ortholog of the zonula occludens (ZO-1) tight junction protein that interacts with Neph1 (Huber et al., 2003), providing strong support for functional conservation of these molecules. The ND controls access of molecules to the labyrinthine channels for uptake by endocytosis, and can discriminate between molecules of different sizes in a rate-dependent manner. Finally, in contrast to that reported by Weavers et al. (Weavers et al., 2009) and reminiscent of their action in the embryonic musculature, Sns and Kirre contribute to the adhesion of the GCNs into an organized garland and their fusion into binucleate cells.

MATERIALS AND METHODS

Fly stocks

The following have been described: $sns^{zf1.4}$ and sns^{XB3} (Bour et al., 2000), *Df(1)w67k30* (Ruiz-Gomez et al., 2000), hbs^{2593}(Artero et al., 2001); *UAS-sns*[*C-HA*], $sns^{zf1.4}$, *UAS-sns*[*C-HA*] and *sns-Gal4* (Kocherlakota et al., 2008). The following were obtained from the indicated stock centers: *twiGal4, UAS-gapGFP* and the balancer stocks *CyO, P{ry*[+*t7.2*]= *en1}wg*[*en11*], *FM7, ftz-lacZ* and *CyO, P{*(*w*[*1mC*]¼*GAL4-twi.G*)*}2.2, P*(*UAS-2xEGFP*)*AH2.2* (Bloomington Stock Center, Bloomington, IL); RNAi stocks for *UAS-kirre-IR*(*1*) (v27227), *UAS-kirre-IR*(*2*) (v3111), *UAS-sns-IR*(*1*) (v877) and *UAS-pyd-IR* (v38863) (Vienna Drosophila RNAi Center, Vienna, Austria). $sns^{4.3}$ includes a V1003E mutation in the fibronectin type III domain. Rare escapers were identified by crossing $sns^{4.3}$, *Act5C-Gal4/CyO* and $sns^{4.3}$, *UAS-2XEGFP/CyO. UAS-sns-IR*(*2*) was generated by insertion of a 712 bp fragment, using primers 5′-GGC-GGCTAGCGACGCTCGCCAGAGGAACCGC-3′ and 5′-GGCGGCTA-GCCCAGGAGGCGCAGGAGCTGAA-3′, into pWIZ. *UAS-kirre*[*C-HA*] was generated by subcloning full-length *kirre* cDNA into pUAST vector, followed by an HA (hemagglutinin) tag at the last amino acid of Kirre. Sns deletions were made using PCR with mismatch oligonucleotides to generate *sns*[*mlg4*] (deletion of aa 396-461) and *sns*[*mIg6*] (deletion of aa 592-664), and then subcloned into pUAST, named as *UAS-sns*[*mIg4*] and *UAS-sns*[*mIg6*]. *UAS-sns*[*mIg4*] and *UAS-sns*[*mIg6*] were recombined with $sns^{zf1.4}$ to rescue *sns* null mutant under the *sns-Gal4* driver. *sns-GCN-Gal4*, *sns-GCN-lacZ* and *sns-GCN-nGFP* were generated by insertion of a 2 kb enhancer from intron 1 into pPTGAL, pH-Pelican and pH-Stinger vectors, respectively. All transgenic stocks were generated by Genetic Services (Cambridge, MA).

Immunohistochemistry and TUNEL detection

Homozygous mutant embryos were identified by the absence of β-galactosidase (Kocherlakota et al., 2008). Primary antibodies to Sns (Bour et al., 2000) (embryos, 1:200, sorted embryonic GCNs, 1:100, larval GCNs, 1:80), Kirre (Galletta et al., 2004) (embryos, 1: 200, sorted embryonic GCNs, 1:100, larval GCNs, 1:1000) anti-β-galactosidase (1:500, Promega, Madison, WI), anti-GFP (1:400, Rockland Immunochemicals, Gilbertsville, PA), and Fasciclin 3 (clone 7G10, 1:10, Developmental Studies Hybridoma Bank) were used in this study. Alexa dye conjugated (1:200, Invitrogen, Carlsbad, CA), and biotin-conjugated (1:200, Vector Laboratories, Burlingame, CA) secondary antibodies were used. Colorimetric detection used the VECTASTAIN Elite ABC Kit (Vector Laboratories) with diaminobenzidine substrate. Apoptotic cells were visualized using the In Situ Cell Death Detection Kit (Roche) according to the manufacturer's instructions. Embryos were imaged using a Zeiss Axioplan, for colorimentric staining, and a Zeiss LSM-510 confocal microscope, for fluorescent staining.

Live imaging

Living embryos were collected, dechorionated, glued onto a coverslip, and immersed in PBS buffer in an Attofluor cell chamber (Molecular Probes, Carlsbad, CA). Images were acquired with a Zeiss LSM510 laser-scanning microscope, Zeiss C-Apochromat 40× 1.20 W Korr UV-VIS-IR objective and an excitation wavelength of 920 nm. Emission was collected using a 495-545 nm band-pass filter. All Z-series time-lapse sequences were taken every 10 minutes, with optical sections captured every 0.8 μm.

Flow cytometry

Embryos aged to 9-12 or 12-18 hours after egg laying (AEL) were collected at 25°C, dechorionated and transferred into Schneider's media, 3 mM EGTA, in a glass homogenizer. Homogenized cells were pelleted (50 ***g***, 2.5 minutes). The cell pellet resuspended (Schneider's media, 3 mM EGTA) added to Histopaque-1077 (Sigma, St Louis, MO) and centrifuged (400 ***g***, 30 minutes). Cells at the interface were collected, washed with media, pelleted (200 ***g***, 5 minutes), resuspended and filtered through a 70 μm filter. Cells were sorted using a MoFlo cell sorter (Dako, Ft Collins, CO). GFP-positive GCNs were incubated on poly-L-lysine coated slides for 30 minutes, fixed with 4% formaldehyde in PBS and stained as above.

Electron microscopy

Dissected GCNs were fixed with 2.5% paraformaldehyde/2% glutaraldehyde/PBS and carried out for TEM with standard techniques. Conventional Immunoelectron microscopy (immunoEM) was done as previously described (Tepass, 1996). The dissected GCNs were prefixed in 8% paraformaldehyde/0.02% glutaraldehyde/PBS, and incubated with primary antibody: anti-Kirre (1:20), anti-Sns (1:5), followed by Nanogold-conjugated secondary antibodies (1:200) (Nanoprobes, Yaphank, NY). After postfixation and silver enhancement, samples were dehydrated, embedded and sectioned. For cryo-immunoEM, the fixed garland cells were embedded in gelatine, cryosectioned and incubated with anti-Kirre or anti-Sns followed by 5 nm or 10 nm gold-conjugated secondary antibody, respectively. All images were acquired on an FEI TEM.

For scanning electron microscopy (SEM), dissected GCNs were fixed in 2.5% glutaraldehyde/2% paraformaldehyde/PBS, washed and treated with 1% Osmium Tetroxide. Following dehydration, samples were incubated in hexamethyldisilazane (Sigma-Aldrich) and air dried overnight. Images were

acquired with Hitachi tabletop electron microscope TM-1000 (Fig. 3D) and an FEI Quanta 600 FEG Extended Vacuum Scanning Electron Microscope (ESEM).

Endocytosis assays

Dissected second-instar GCNs were incubated with Shields and Sang M3 Insect Medium containing 1 mg/ml Cascade Blue dextran 10 kD and either 50 μg/ml Alexa Fluor 555 BSA or 1 mg/ml fluorescein dextran 500 kD (Molecular Probes) for 30 seconds or 5 minutes at 25°C as indicated. Cells were washed with ice-cold PBS for 30 minutes, and fixed with 4% paraformaldehyde/PBS for 10 minutes. Cells were rinsed, mounted and imaged using a Zeiss LSM510 confocal microscope. Uptake efficiency was quantitated by calculating the fluorescence intensity per μm^2 of a single confocal section at the cell midpoint with Axiovision 4.7.

Statistical analysis

Cells and nuclei were manually quantitated from confocal Z-series. NDs were counted for one TEM traverse section per cell. Analysis of variance (ANOVA) was used for multiple comparisons. Student's *t*-test was used to determine the statistical significance between two interventions. A statistically significant difference was defined as $P<0.05$.

RESULTS

The IgSF proteins Sns and Kirre are expressed in the GCNs

Published studies and our unpublished observations noted the presence of the *kirre* and *sns* transcripts in the developing GCNs of late-stage embryos. We therefore examined these embryos using antisera against Kirre and Sns to confirm that the encoded proteins were indeed present in the GCNs. It was also of interest to determine whether these proteins were expressed in different populations of cells, as in the developing musculature, or co-expressed within single nephrocytes, as observed for their orthologs in the mammalian kidney. GCNs were identified deep inside the embryo using *sns-GCN-lacZ*, a transgene in which expression of β-galactosidase was under control of an *sns* enhancer element (Fig. 1B). Immunostaining with antisera against β-gal and Sns or Kirre revealed expression of both proteins in the GCNs at stage 13 (Fig. 1C-F), when they are still mononucleate, and stage 16, when most GCNs are binucleate (Fig. 1G-L). Expression was apparent at points of cell-cell contact, consistent with a model in which the earliest expression of Kirre and Sns mediates adhesion between these cells. By stage 16, Sns remained enriched at points of cell-cell contact and became clearly visible in regions of the cell surface that are not in direct contact with other cells (Fig. 1G-I). This pattern was not uniform, possibly prefiguring the later pattern of ND channels on the cell surface. Kirre also remained enriched at points of cell-cell contact, and became visible at the cell surface in a somewhat more punctuate pattern (Fig. 1J-L). Lastly, whereas Sns and Kirre mark different myoblast populations in the embryonic musculature and mediate adhesion between these cell types, they were co-expressed in the GCNs (Fig. 1M-T). To ensure that co-expression was not a result of fusion, embryos transgenic for *sns-GCN-nGFP* were lightly homogenized and the disrupted cells sorted by fluorescence-activated cell sorting (FACS). They were then immunostained to visualize Kirre and Sns. Notably, all 39 mononucleate GFP-positive cells identified in this analysis expressed Sns and 37/39 cells expressed Kirre. With the cells, one could observe regions of Sns and Kirre co-localization and non-co-localization in both mononucleate (Fig. 1M-P) and binucleate GCNs (Fig. 1Q-T). We therefore conclude that the mononucleate GCNs co-express Sns and Kirre, analogous to co-expression of Nephrin and Neph1 in podocytes in the kidney.

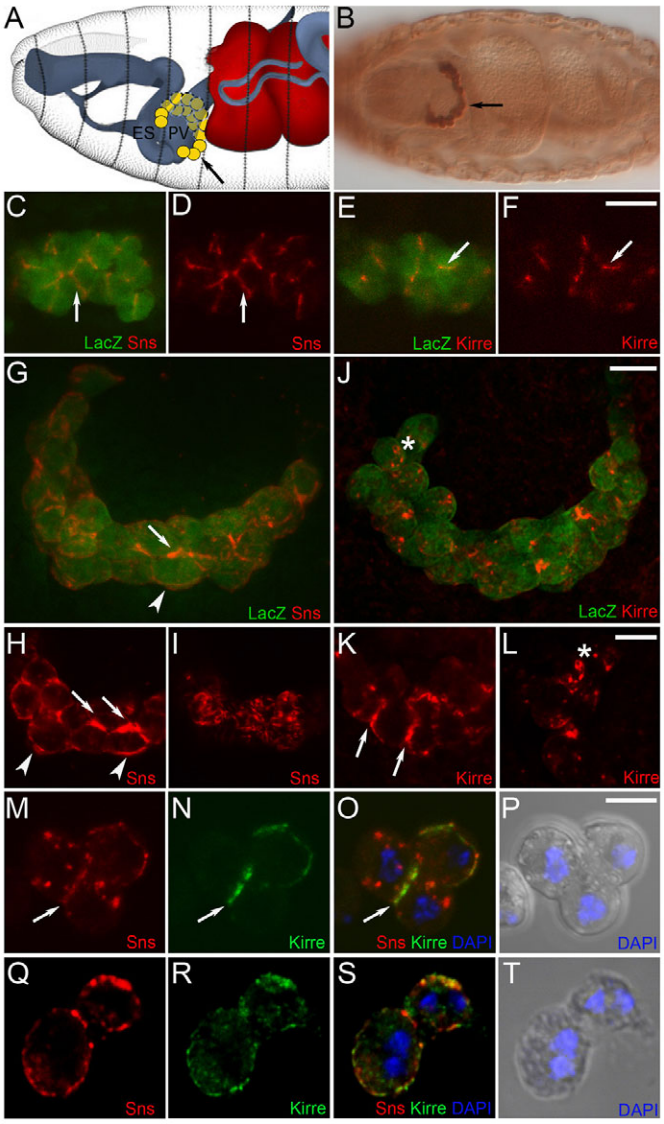

Fig. 1. Expression of Sns and Kirre in embryonic GCNs. (**A**) Schematic, modified with permission from Hartenstein (Hartenstein, 1993) to indicate the position of GCNs (yellow) at embryonic stage 16. (**B-L**) GCNs were identified by expression of the *sns-GCN-lacZ* transgene. (B) Ventral view, stage 16. (C-F) Confocal single section of GCNs at stage 13. Sns (red) and Kirre (red) are present at cell-cell contacts (arrows). Arrow in B indicates GCNs marked by β-galactosidase. (G-L) Ventral views, stage 16. Projections of confocal sections (~20 μM) (G,J) and single sections (H,I,K,L) reveal Sns (H,I) and Kirre (K,L) on the cell surface (arrowheads), cell-cell contacts (arrows) and in intracellular and cell surface puncta (asterisks). Note the uneven pattern of Sns on the cell surface in (I). (**M-T**) FACS-isolated nGFP-positive cells from *sns-GCN-nGFP* transgenic embryos. Single confocal sections show partial co-localization of Sns and Kirre on the surface of mononucleate (9-12 hours AEL) (M-P) and binucleate (12-18 hours AEL) (Q-S) GCNs. Scale bars: 10 μm in C-L; 5 μm in M-T. ES, esophagus; PV, proventriculus.

Binucleate GCNs are generated by fusion that is mediated, at least in part, by the IgSF proteins Sns, Hbs, Kirre and Rst

As cited above, Kirre and Sns direct fusion that generates multinucleate muscle precursors and muscle fibers. To determine whether these proteins serve a similar purpose in the GCNs, and the

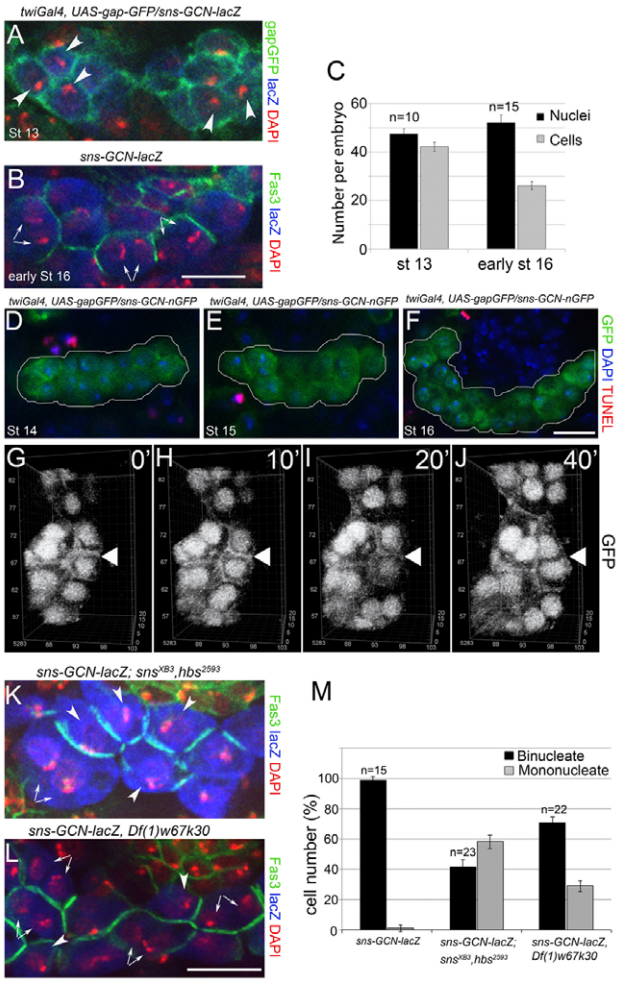

Fig. 2. IgSF proteins contribute to fusion of mononucleate GCNs. (**A**,**B**) GCNs in fixed transgenic embryos labeled with antibodies to *sns-GCN-lacZ* (blue, A,B), *twiGal4* driven *UAS-gapGFP* (A) and anti-Fas3 (B) for the cell membranes (green); DAPI marks nuclei (red, A,B). (A) Stage 13, mononucleate GCNs (arrowheads); (B) early stage 16, binucleate GCNs (arrows). (**C**) Quantitation of cell and nuclei number; *n* equals embryos analyzed. The number of GCNs decreases significantly between stage 13 and early stage 16 ($P<0.001$), the number of nuclei remains essentially the same ($P=0.03$). Bars show mean±s.e.m. (**D-F**) Apoptotic GCNs are not detected. GCNs from transgenic *sns-GCN-nGFP* (anti-GFP, green) embryos identified at stages 14-16, apoptosis identified by TUNEL staining (red). (**G-J**) Time-lapse imaging of cell fusion over a 40-minute period in stage 14 embryos, as revealed by *sns-GCN-nGFP* and *twiGal4* driven *UAS-gapGFP*. The white triangle denotes membrane breakdown (see Movie 1 in the supplementary material; scale units in μm). (**K-M**) Binucleate (arrows) and mononucleate (arrowheads) GCNs are present in (K) homozygous sns^{xb3}, hbs^{2593} and (L) hemizygous *Df(1)w67k30*, which removes *kirre* and *rst*, early stage 16 embryos. Mutant and control embryos express *sns-GNC-lacZ* (anti-β-gal, blue), anti-Fas3 staining the cell membrane (green), and DAPI staining the nuclei (red). (M) Quantitation of bi- and mononucleate cells, where *n* equals embryos analyzed. Bars show mean±s.e.m. There is a significant decrease of binucleate GCNs in the mutant samples compared with wild-type control ($P<0.001$). Scale bars: 10 μm.

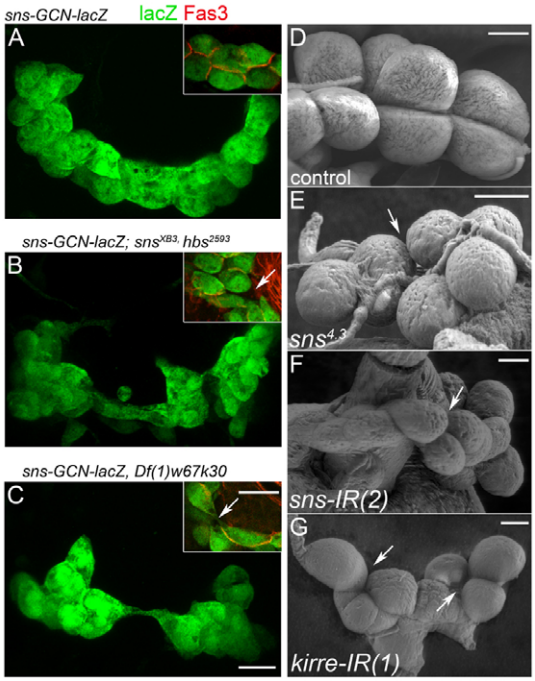

Fig. 3. IgSF proteins mediate GCN adhesion and shape of embryonic and larval GCNs. (**A-C**) Confocal projections (approx. 25 μm) of ventral views of GCNs identified by *sns-GCN-lacZ* (green) at stage 16; cell membranes are marked by anti-Fas3 (red; inset). Compared with control GCNs (A), the GCNs of embryos mutant for sns^{XB3}, hbs^{2593} (B) or hemizygous for *Df(1)w67k30* (C) are disorganized, misshapen and more loosely associated (arrows). (**D-G**) SEMs of third-instar larval GCNs from *sns-GCN-nGFP* (D), $sns^{4.3}$ (E), *sns-GCN-nGFP, sns-GCN-Gal4/+; UAS-sns-IR(2)/+* (F) and *sns-GCN-Gal4/UAS-kirre-IR(1)* (G). Defects similar to those in B and C are apparent (arrows). Scale bars: 10 μm.

binucleate GCNs are a consequence of cell fusion, we examined the cells at embryonic stage 13, when most are mononucleate (Fig. 2A), and stage 16, when most had become binucleate (Fig. 2B). Quantitation revealed approximately 50 nuclei at each stage, but a decline in the number of cells from 42 to 26 (Fig. 2C). These data are consistent with the generation of binucleate cells by fusion. To confirm that the decrease in cell number was due to fusion, and not a combination of cell death and nuclear division, the GCN cluster was examined for the presence of dying cells using terminal deoxynucleotidyl transferase-mediated dUTP nick-end labeling (TUNEL) (Fig. 2D-F). Representative images reveal the presence of TUNEL-positive, non-nGFP-positive cells in the surrounding tissues but no TUNEL-positive nGFP-positive, GCNs. In addition, time-lapse imaging of GCNs expressing *sns-GCN-nGFP* and *UAS-gapGFP* driven by *twiGal4* further confirmed that binucleate GCNs can form by fusion (Fig. 2G-J; see Movie 1 in the supplementary material).

Next it was of interest to determine whether Sns and Kirre, or their paralogs Hbs and Rst, contribute to this fusion event. Previous studies have shown that Kirre and Rst serve redundant roles in the founder myoblasts (Strunkelnberg et al., 2001), and Sns and Hbs are both competent to direct the initial fusion event between fusion competent myoblasts and founder cells (Menon et al., 2005; Shelton et al., 2009). Whereas Rst expression has not been detected in the GCNs, we have observed significant expression of Hbs (data not shown). To assess their role in fusion of GCNs, the *sns-GCN-lacZ* transgene was recombined into fly stocks mutant for both *sns* and *hbs*, or having a deficiency that removes both *kirre* and *rst*. The number of binucleate and mononucleate GCNs was then quantitated and compared in these mutant embryos. In contrast to wild-type embryos, in which 99.6 percent of the *sns-GCN-lacZ*-positive cells

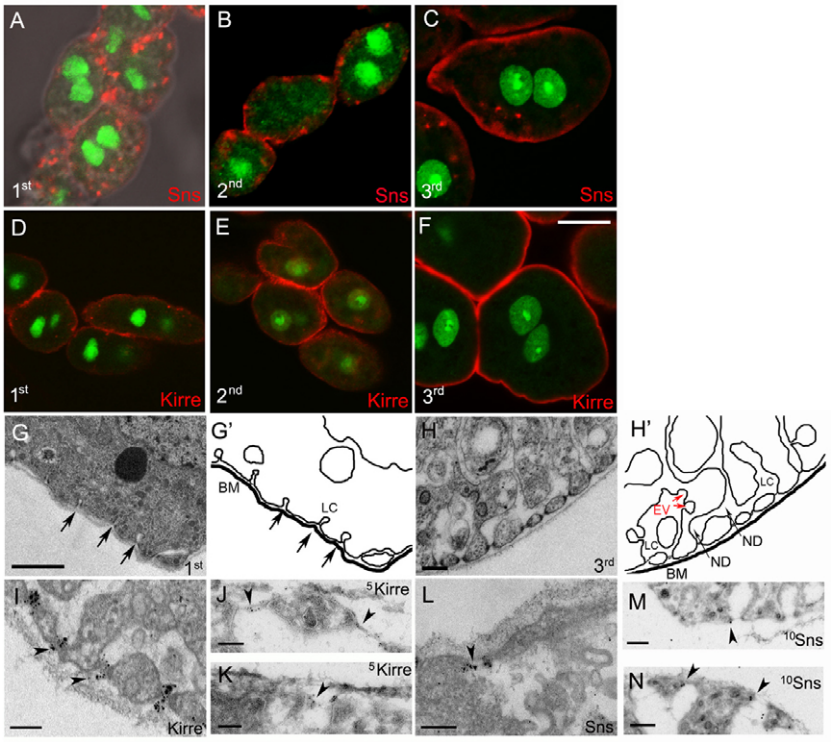

Fig. 4. Sns and Kirre localize to the ND in larval GCNs. GCNs dissected from larvae transgenic for *sns-GCN-nGFP* at first, second and third-instar larvae. (**A-F**) Single confocal sections of GCNs were immunostained with anti-GFP (green) and anti-Sns (A-C, red) or anti-Kirre (D-F, red). (**G-H'**) TEM and corresponding schematic of the cortical region of GCNs from first (G) or third (H) instar larvae. The labyrinthine channels (LC) are apparent and endocytic vesicles noted (EV). Arrows denote the NDs. (**I-N**) ImmunoEM reveals Kirre in the ND of GCNs from third-instar larvae (I-K, arrowheads) and Sns in the ND of GCNs from second (L) and third (M,N) instar larvae (arrowheads). (I,L) Conventional immunoEM; (J,K,M,N) cryo-immunoEM. Scale bars: 10 μm in A-F; 1 μm in G; 200 nm in H,M,N; 100 nm in I-K. BM, basement membrane.

were binucleate by early stage 16, almost 60% of the cells lacking both *sns* and *hbs* remained mononucleate (Fig. 2K,M). A lower percentage of cells remained mononucleate when lacking only *sns* and no mononucleate cells were observed in the absence of *hbs* (data not shown), suggesting that these proteins have some redundancy of function in directing GCN fusion, and observed for myoblast fusion. In comparison, approximately 30% of the GCNs in embryos lacking *kirre* and *rst* remained mononucleate (Fig. 2L,M). We conclude that the IgSF proteins contribute to GCN fusion, but are not absolutely essential for the presence of binucleate cells.

Sns and Kirre mediate adhesion between GCNs, and formation of a structure reminiscent of the mammalian slit diaphragm

The above observations suggest that the abilities of Sns, Hbs, Kirre and Rst to direct myoblast fusion have been retained in GCNs. The roles of these proteins in directing adhesion between myoblasts have also been retained. Indeed, the GCNs in embryos lacking either *sns* and *hbs* or *kirre* and *rst* are misshapen compared with their spherical wild-type counterparts and do not adhere well to each other (Fig. 3A-C). These shape defects and loose association are also characteristic

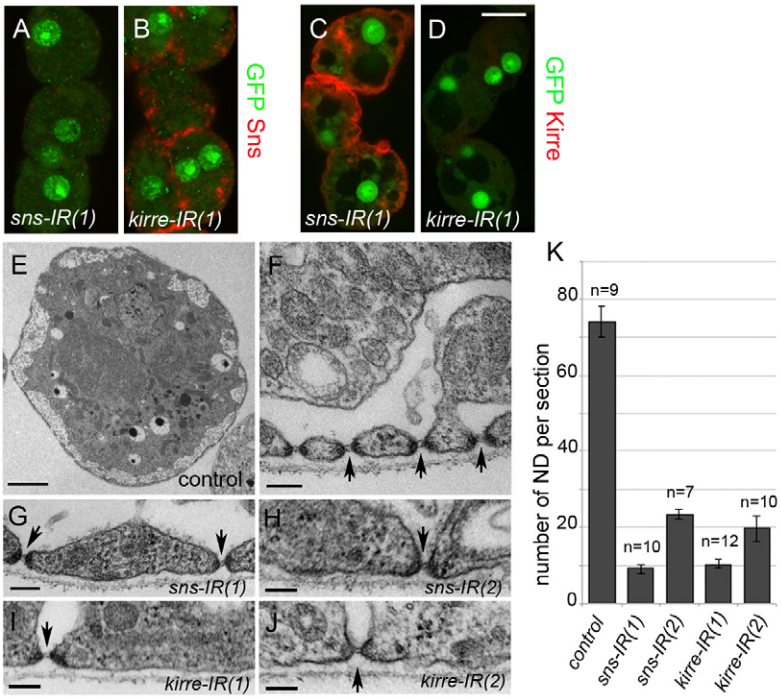

Fig. 5. Sns and Kirre are required for formation and/or maintenance of the ND. (**A-D**) GCNs from *sns-GCN-nGFP, sns-GCN-Gal4/+; UAS-sns-IR(1)/+* (A,C) or *sns-GCN-nGFP, sns-GCN-Gal4/UAS-kirre-IR(1)* (B,D) second-instar larvae were immunostained for Sns (A,B) or Kirre (C,D). (**E-J**) TEM of the cortical region of GCNs from second-instar larvae. (E,F) GCNs from *sns-GCN-nGFP, sns-GCN-Gal4/+* second-instar larvae are regarded as the wild-type control and show the transverse section (E). The NDs are apparent, along with double membrane at entry site (arrows). (G-J) The number of NDs is decreased upon knockdown of Sns or Kirre in larvae genetically *sns-GCN-nGFP, sns-GCN-Gal4/+;UAS-sns-IR/+* or *sns-GCN-nGFP, sns-GCN-Gal4/UAS-kirre-IR*, but remaining NDs appear to be normal. (**K**) Quantitation of NDs from above genotypes, bars show mean±s.e.m. Scale bars: 10 μm in A-D; 2 μm in E; 100 nm in F-J.

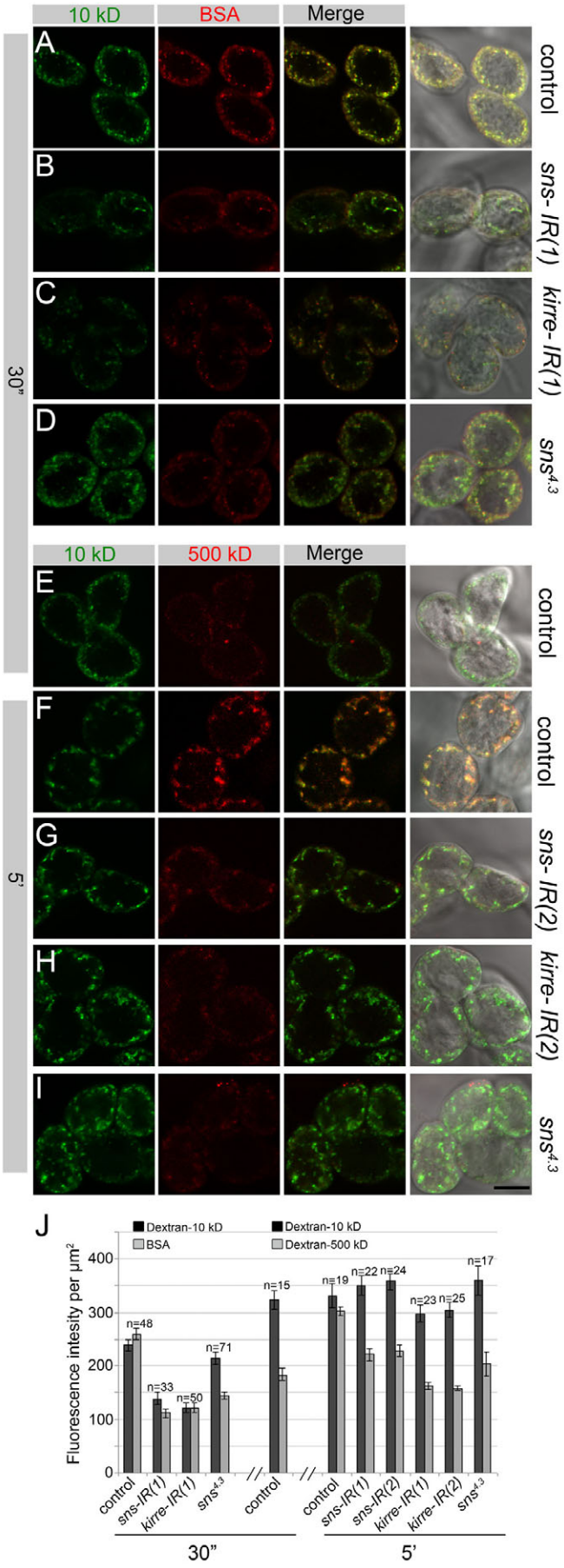

Fig. 6. Sns and Kirre mediate uptake of molecules by endocytosis. GCNs from second-instar larvae were incubated with Cascade Blue dextran 10 kD and either Alexa Fluor 555 BSA for 30 seconds (**A-D**), or fluorescein dextran 500 kD for 5 minutes (**E-I**). GCNs were genetically *sns-GCN-Gal4/+* (A,E,F), *sns-GCN-Gal4/+; UAS-sns-IR*(*1*) or (*2*)/+ (B,G), *sns-GCN-Gal4/UAS-kirre-IR*(*1*) or (*2*) (C,H) or $sns^{4.3}/sns^{4.3}$ (D,I). Uptake of both dextran 10 kD (green) and BSA (red) are reduced upon knockdown of Sns or Kirre, or in a hypomorph of *sns* upon incubation for 30 seconds. After incubation for 5 minutes, however, only uptake of dextran 500 kD is reduced by Sns or Kirre knockdown. (**J**) Quantitation of fluorescence intensity per μm^2, where *n* equals the number of cells analyzed. Bars show mean±s.e.m. Scale bar: 10 μm.

of larval GCNs in which Sns or Kirre has been decreased by RNAi (Fig. 3F,G). In contrast to null alleles of sns, which die during embryogenesis due to the absence of muscle fibers (Bour et al., 2000), a small number of embryos mutant for $sns^{4.3}$, a hypomorphic allele with an ethyl methanesulfonate-induced point mutation in the extracellular fibronectin type III-binding domain, survived to pupal development and their GCNs could be analyzed in third-instar larvae (Fig. 3E). In contrast to the tighter association of wild-type GCNs, these cells often broke apart upon dissection (data not shown).

Consistent with a model in which maintenance of the 'garland' requires Sns and Kirre, GCNs from first, second and third-instar larvae continued to express Sns and Kirre proteins (Fig. 4A-F). Both proteins became more strongly and uniformly expressed at the cell surface with passage into the third-instar larval stage. The labyrinthine channels, sites of high endocytic activity associated with detoxification, appeared to form by invagination and adhesion between two closely spaced regions of the plasma membrane in GCNs from first instar larvae (Fig. 4G). As the cells grew in size and differentiated in second- and third-instar larvae, the channels became more elaborate and associated with a higher number of endocytic vesicles. Notably, the access point between the channels and hemolymph (the ND) appeared remarkably similar to the SD in the mammalian kidney (Fig. 4H) (Wartiovaara et al., 2004). The diameter of the NDs in GCNs from third-instar larvae averaged 29.7 nm (±1.06 s.e.m.), which is similar to the 35-40 nm reported for the SD in vertebrates (Ruotsalainen et al., 1999; Wartiovaara et al., 2004). Notably, similar immunoEM analysis revealed that Sns and Kirre were associated with the ND entry point into the labyrinthine channels, in samples processed by conventional immunoEM (Fig. 4I,L) or cryo-immunoEM (Fig. 4J,K,M,N).

Sns and Kirre are essential for formation and/or maintenance of the ND, and uptake of molecules into the labyrinthine channels for processing by endocytosis

To address whether *sns* or *kirre* is necessary within the GCNs for formation of the ND, flies transgenic for *sns-GCN-Gal4* were used to direct expression of UAS-*sns RNAi* (*sns-IR*) transgenes or UAS-*kirre RNAi* (*kirre-IR*) transgenes. We carried out TUNEL analysis of GCNs dissected from third-instar larvae to evaluate their viability. Whereas Weavers et al. (Weavers et al., 2009) noted a decrease in the number of GCNs in larvae lacking Kirre, our quantitation revealed that the viability of approximately half of the cells was seriously impaired by the absence of Sns or Kirre (see Fig. S1 and Table S1 in the supplementary material). By comparison, GCNs from second instar larvae expressing these RNAi transgenes were not detectable

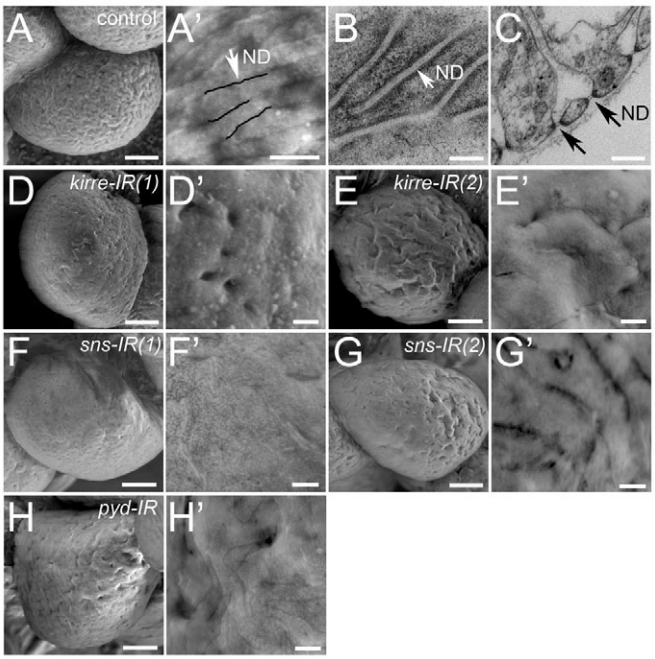

Fig. 7. SEM analysis of the GCN surface reveals smoothening that is coincident with a decline in NDs. SEM analysis of GCNs from *sns-GCN-nGFP, sns-GCN-Gal4/+* (**A-C**), *sns-GCN-nGFP, sns-GCN-Gal4/UAS-kirre-IR(1)* (**D**,**D′**), *sns-GCN-nGFP, sns-GCN-Gal4/UAS-kirre-IR(2)* (**E**,**E′**), *sns-GCN-nGFP, sns-GCN-Gal4/+; UAS-sns-IR(1)/+* (**F**,**F′**), *sns-GCN-nGFP, sns-GCN-Gal4/+; UAS-sns-IR(2)/+* (**G**,**G′**) and *sns-GCN-nGFP, sns-GCN-Gal4/UAS-pyd-IR* (**H**,**H′**) third-instar larvae. (A′,B,C) Note the NDs on the GCNs surface. Scale bars: 5 μm in A,D-I; 1 μm in D′-I′; 500 nm in A′; 100 nm in B,C.

by TUNEL and exhibited normal morphology (data not shown). We therefore focused our Sns and Kirre RNAi analysis on cells at this earlier stage to ensure that any observed defects were not a consequence of apoptosis. Sns was no longer detectable in GCNs expressing *sns-IR*, but the level of Kirre protein remained fairly robust (Fig. 5A,C). Similarly, Kirre protein was no longer detectable in GCNs expressing *kirre-IR* but Sns remained easily detectable (Fig. 5B,D). Most notably, TEM analysis revealed that *sns-IR* and *kirre-IR* have a dramatic impact on the number of NDs (Fig. 5K). The NDs that did form appeared to be normal by TEM (Fig. 5E-J) and did not differ significantly from wild type in diameter. From these data we conclude that Sns and Kirre are instrumental in the formation of the ND.

One hallmark of the GCNs is their high levels of endocytosis from sites deep within the labyrinthine channels, of hemolymph components that are thought to enter the channels by passage through the ND. Given the dramatic decrease in the number of NDs upon knockdown of Sns or Kirre by RNAi, we examined the ability of molecules of different sizes to enter the cell. We again used GCNs from second instar larvae to avoid potential complications of dying GCNs in third-instar larvae. Wild-type, $sns^{4.3}$, *sns-IR* and *kirre-IR* GCNs were co-incubated with Alexa Fluor 555 BSA and dextran 10 kD for 30 seconds. Tracers of both sizes were taken up efficiently in the wild-type control, and fluorescence was apparent in the membrane proximal, cortical region (Fig. 6A). By contrast, uptake of both tracers was reduced upon knockdown by *sns-IR* (Fig. 6B) or *kirre-IR* (Fig. 6C). Though uptake of dextran 10 kD was not severely reduced in GCNs homozygous for $sns^{4.3}$, these cells did exhibit reduced uptake of BSA (Fig. 6D). GCNs of the same genotypes were also co-incubated with Cascade Blue dextran 10 kD and fluorescein dextran 500 kD. In the control samples, the dextran 10 kD tracer was taken up efficiently upon incubation for either 30 seconds (Fig. 6E) or 5 minutes (Fig. 6F) as expected. However, the level of uptake of the dextran 500 kD tracer increased significantly upon incubation for 5 minutes relative to 30 seconds (Fig. 6E,F). Thus, the ND can distinguish between molecules of different sizes, such that larger molecules are taken up more slowly. Surprisingly, whereas dextran 10 kD was not taken up efficiently in a 30 second incubation with *sns-IR* or *kirre-IR* cells, it was taken up efficiently in all cells upon incubation for 5 minutes, independent of the presence of *sns-IR* or *kirre-IR* (Fig. 6F-H). The dextran 500 kD tracer, by contrast, which was taken up well in the 5 minute control (Fig. 6F), was taken up very poorly upon knockdown by *sns-IR* (Fig. 6G), *kirre-IR* (Fig. 6H) or in GCNs homozygous for $sns^{4.3}$ (Fig. 6I). Thus, the ND is essential for entry of BSA or dextran 500 kD into the cell. Moreover, large molecules pass through the ND at very reduced rates compared with small molecules. To ensure evaluation of passage through the ND, and not simply endocytosis, the fluorescence intensity per μm^2 was quantitated (Fig. 6J). We note also that the dextran 10 kD and either BSA or dextran 500 kD co-localize in puncta within the cell (Fig. 6; see Movie 2 in the supplementary material), suggesting that they are taken up by the same mechanism under wild-type conditions. We also note that the limited amount of tracer taken up upon *sns-IR* or *kirre-IR* knockdown appears to be properly endocytosed, as evidenced by their appearance in characteristic intracellular puncta. Thus, these cells do not appear to be defective in endocytosis per se but, rather, in the process through which large fluorescent tracers enter the channels for subsequent endocytosis. We conclude from these data that NDs are essential for large molecules to pass from the hemolymph into the labyrinthine channels for endocytosis. By comparison, either small molecules have an alternative mechanism for uptake that can compensate for a decrease in NDs, or they are able to pass through the ND more readily than large molecules, eventually allowing efficient uptake even under conditions in which the number of NDs is limited.

Perturbation of the ND by *pyd-IR* or mutation of the Sns extracellular domain

Analysis of GCNs from third-instar larvae by SEM revealed a physically uneven cell surface covered with long furrows (Fig. 7A,A′). The spatial characteristics of these furrows matched the ND diameter and the overall distance between NDs seen in TEM analysis that skimmed the cell surface (Fig. 7B) or traversed the cell diameter (Fig. 7C). Thus, the ND array is visible by SEM analysis of the cell surface. To confirm this conclusion, the surface of GCNs from third-instar larvae expressing either *kirre-IR(1)*, *kirre-IR(2)*, *sns-IR(1)* or *sns-IR(2)* were examined (Fig. 7D-G′). The surface was more uniform in these GCNs, consistent with the decrease in NDs. We then examined the impact of Pyd knockdown on the appearance of ND furrows to determine whether this *Drosophila* protein, like its mammalian counterpart, contributed to ND function. *Pyd-IR* clearly perturbed the formation of ND furrows on the cell surface (Fig. 7G). These data suggest that *pyd* may function in a manner reminiscent of its mammalian ortholog ZO-1.

We then examined the impact on the ND of overexpression of Sns or Kirre, or mutation of the Sns extracellular domain. For comparison, a typical ND cross section is seen in Fig. 8A. Whereas most NDs were normal in appearance, a small percentage of NDs [6 out of 103 (5.8%), collected from 16 GCNs] exhibited an extended region of attachment upon overexpression of Sns (Fig. 8B). No structures of this type were apparent upon overexpression of Kirre

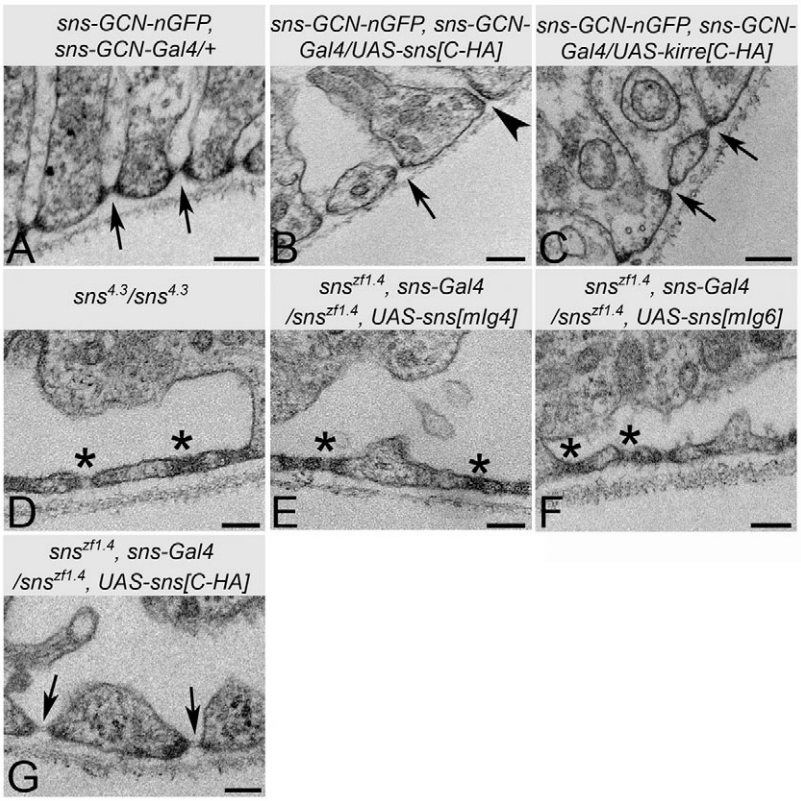

Fig. 8. ND structure is perturbed by overexpression, mutation and deletion of Sns extracellular domains. TEM analysis of GCNs from second- (**D-G**) and third- (**A-C**) instar larvae. Rare examples of expanded NDs were observed upon overexpression of Sns (B, arrowhead) but not Kirre (C, arrow). Defective NDs seen in GCNs from a hypomorph of *sns* (D) or upon rescue with Ig4- or Ig6-deleted Sns (E,F; asterisk), but not with full-length Sns (G, arrow). Scale bars: 100 nm.

(0 out of 79 NDs, collected from 18 GCNs) (Fig. 8C). The ND structure was then examined in GCNs homozygous for the hypomorphic allele $sns^{4.3}$. Whereas electron-dense regions characteristic of NDs were apparent in the plasma membrane just under the basement membrane (Fig. 8D), the structure itself was abnormal. We have found that Ig domains 4 and 6 are not required for muscle development, and embryos homozygous for null alleles of *sns* can be rescued by expression of Sns lacking these domains (data not shown). Therefore, the GCNs from these rescued third-instar larvae could be analyzed by TEM. As observed in $sns^{4.3}$, the ND structure of these GCNs was abnormal, with an extended electron-dense region that did not resolve. The uptake of molecules into these cells was disrupted but variable (data not shown), necessitating further study. We conclude from these data, however, that the fibronectin type III-binding region, Ig4 and Ig6 of Sns are essential for the ND to assemble the correct structure, probably by mediating crucial protein-protein interactions.

DISCUSSION

Our data and other recent studies (Weavers et al., 2009) demonstrate that the GCNs have significant structural and functional similarities to podocytes in the mammalian kidney. Sns and Kirre are instrumental in directing and/or stabilizing interactions at sites of membrane invagination that become the NDs. These proteins parallel the role of their mammalian orthologs Nephrin and Neph1 in the SD that forms between podocyte foot processes in the kidney glomerulus. In addition, Sns and Kirre mediate tight adhesion between GCNs in the embryo, and, in contrast to Weavers et al. (Weavers et al., 2009), we note that these proteins also direct GCN fusion. Both proteins are expressed during larval life and we note significant cell death in their absence. Sns clearly plays a specific structural role in the ND that is perturbed by mutations in its extracellular domain. Finally, the SD and ND both mediate the flow of molecules between the circulatory system and the excretory system, and appear to discriminate between molecules on the basis of size and rate of passage.

The insect slit diaphragm

The GCNs are thought to process waste material and detoxify the insect hemolymph, its open circulatory system, through a process of endocytosis and degradation (Aggarwal and King, 1967; Crossley, 1985). Endocytosis occurs from sites deep within labyrinthine channels that form by invagination of the plasma membrane (Koenig and Ikeda, 1990), and proteins associated with endocytosis localize to the cortical region of the cytoplasm in membranes associated within these channels (Halachmi et al., 1995). The channels and associated membranes expand in mutants that block endocytosis (Kosaka and Ikeda, 1983), and compounds such as horseradish peroxidase (Chang et al., 2002), dye-conjugated BSA or avidin (Chang et al., 2002), and various dextrans (Rusten et al., 2006), readily pass through the plasma membrane into these channels. Access appears to occur through a structure that is reminiscent of the SD in vertebrates (Koenig and Ikeda, 1990; Kosaka and Ikeda, 1983). We have shown that this nephrocyte diaphragm is dependent on the presence of Sns and Kirre, and that perturbation of the Sns extracellular domain causes obvious defects in the ND. Thus, IgSF homologs appear to be a structural component of this access point in both insects and vertebrates.

The number of NDs decreases significantly upon knockdown of Sns or Kirre, but a small number still remain. The uptake of large molecular tracers is severely diminished under these conditions, suggesting that the NDs are a major route of access to the endocytic machinery within the labryinthine channels. Perhaps more revealing

relative to the initial findings of Weavers et al. (Weavers et al., 2009), we find that the uptake of small molecules is slower under conditions of Sns or Kirre knockdown but ultimately achieves normal levels. Thus, like the SD, the ND appears to be more permeable to small molecules. Interestingly, studies in vertebrates have addressed the relative contributions of the podocyte basement membrane and the slit diaphragm to glomerular permeability (e.g. Liu et al., 2003), and found Nephrin and Neph1 to be crucial. Moreover, electron tomography has identified Nephrin as a decisive determinant for filtration of molecules larger than BSA (Wartiovaara et al., 2004).

Parallel molecular interactions?

Nephrin and Neph1 are capable of forming both homodimers and heterodimers, and these abilities could reflect interactions that occur in vivo in cis and/or in trans (Gerke et al., 2003). The diameter of the vertebrate SD is consistent with a model in which this distance could be spanned by homophilic interaction of Nephrin or heterophilic interaction between Neph1 and Nephrin in trans (Ruotsalainen et al., 1999; Wartiovaara et al., 2004). The similar diameter of the *Drosophila* ND therefore supports a model in which interactions between the Kirre and Sns ectodomains determine this distance. The exact molecular interactions remain to be determined, however, and may differ in vertebrates and *Drosophila*. For example, Nephrin is capable of homophilic interactions in trans (Ruotsalainen et al., 1999; Tryggvason, 1999; Tryggvason et al., 1999), a property that Sns does not appear to have (Galletta et al., 2004). Thus, it seems unlikely that Sns spans this distance, as suggested for Nephrin (Khoshnoodi et al., 2003; Patrakka and Tryggvason, 2007; Wartiovaara et al., 2004). Homophilic interactions of Kirre, which can occur (Galletta et al., 2004), could serve this purpose. One might then predict the spacing to be decreased from the observed 30-35 nm due to the shorter extracellular domain of Kirre. Of note, kinetic studies in *Drosophila* S2 cells indicate a strong preference for interaction with Sns (Galletta et al., 2004). Moreover significant levels of Sns or Kirre remain in GCNs from second instar larvae upon knockdown of the corresponding partner, yet the number of NDs is diminished. Localization of each protein by immunoEM analysis under these conditions may prove to be illustrative in this regard. Given the above interaction studies and fact that both proteins are continuously present in the GCN, we tend to favor a model in which heterotypic interactions are preferred as in the embryonic musculature (reviewed by Abmayr et al., 2005; Abmayr and Kocherlakota, 2005). One fundamental difference between Sns and Kirre in the embryonic musculature and the GCNs is that they are expressed in different myoblast cell types but co-expressed within individual garland cells. However, their co-expression in GCNs is another feature in common with Nephrin and Neph1 in vertebrate podocytes.

It is unclear whether Sns and Kirre function through interactions with signal transduction components that parallel those of Nephrin and Neph1 in the GCNs. Signaling molecules thought to be downstream of Sns and/or Kirre in the musculature, and known to be downstream of Nephrin, include N-WASp and components of the Arp2/3 pathway (Berger et al., 2008; Kim et al., 2007; Lu et al., 1997; Richardson et al., 2007; Rohatgi et al., 2001). One other functional parallel between the SD and ND is that of the tight junction protein Pyd, which contributes to formation of ND-associated furrows on the surface of the GCN. Although Pyd interacts biochemically with two different forms of Kirre (Weavers et al., 2009), it remains to be shown whether this interaction occurs through postsynaptic density-95/disks large/zonula occludens-1 (PDZ)-binding sites in Kirre, as observed for binding of its vertebrate counterpart ZO-1 to Neph1 (Huber et al., 2003; Ruotsalainen et al., 2000).

Binucleate nephrocytes, cell fusion and cell division without cytokinesis

GCNs become binucleate before or immediately after their assimilation into the garland of cells that surrounds the esophagus at its junction with the proventriculus. This binucleate nature seems almost invariant, with cells rarely remaining mononucleate or having more than two nuclei. Although an explanation for this invariance is not apparent, the cell appears to accommodate multiple processes to ensure it. Quantitation of cells and nuclei over time, the absence of dying GCNs, and time-lapse imaging suggest that cell fusion is the primary mechanism utilized by wild-type GCNs, and that the IgSF proteins contribute to this process. Some mutant cells are still binucleate, but we cannot eliminate the possibility that other molecules contribute to GCN fusion or that these IgSF proteins function in yet more redundant ways to drive this fusion. Perhaps a drive to become binucleate has forced the cell to compensate for defects in fusion in other ways, such as cell division without cytokinesis. Although all efforts to address such a mechanism have yielded negative results, behavior of this type may be another common property between insect garland cell nephrocytes and mammalian podocytes (Nagata et al., 1995).

Acknowledgements

We thank M. Baylies for the hbs^{2593} allele and the sns^{xb3}, hbs^{2593} recombinant stock. We thank Louis Ross and Cheryl Jensen from the University of Missouri, Columbia, Electron Microscopy Core Facility. We thank the Stowers Institute Cytometry and Imaging core facilities for assistance, in particular Dr Jeff Haug and Mr Danny Stark. We are grateful to Dr Hua Li for help with the statistical analysis. We thank H. Skaer for communicating results in advance of publication. This work was supported by the Stowers Institute for Medical Research and, indirectly, by an NIH R01 award to S.M.A. Deposited in PMC for release after 12 months.

Supplementary material

Supplementary material for this article is available at
http://dev.biologists.org/cgi/content/full/136/14/2335/DC1

References

Abmayr, S. M. and Kocherlakota, K. S. (2005). Muscle morphogenesis: the process of embryonic myoblast fusion. In *Muscle Development in Drosophila* (ed. H. Sink), pp. 92-103. New York: Springer Science and Business Media.

Abmayr, S. M., Balagopalan, L., Galletta, B. J., Hong, S. J., Lawrence, I. G., Kostas, I. and Sarjeet, S. G. (2005). Myogenesis and muscle development. In *Comprehensive Molecular Insect Science*, pp. 1-43. Amsterdam: Elsevier.

Aggarwal, S. K. and King, R. C. (1967). The ultrastructure of the wreath cells of Drosophila melanogaster larvae. *Protoplasma* **63**, 343-352.

Artero, R. D., Castanon, I. and Baylies, M. K. (2001). The immunoglobulin-like protein Hibris functions as a dose-dependent regulator of myoblast fusion and is differentially controlled by Ras and Notch signaling. *Development* **128**, 4251-4264.

Bao, S. and Cagan, R. (2005). Preferential adhesion mediated by Hibris and Roughest regulates morphogenesis and patterning in the Drosophila eye. *Dev. Cell* **8**, 925-935.

Barletta, G. M., Kovari, I. A., Verma, R. K., Kerjaschki, D. and Holzman, L. B. (2003). Nephrin and Neph1 co-localize at the podocyte foot process intercellular junction and form cis hetero-oligomers. *J. Biol. Chem.* **278**, 19266-19271.

Benzing, T. (2004). Signaling at the slit diaphragm. *J. Am. Soc. Nephrol.* **15**, 1382-1391.

Berger, S., Schafer, G., Kesper, D. A., Holz, A., Eriksson, T., Palmer, R. H., Beck, L., Klambt, C., Renkawitz-Pohl, R. and Onel, S. F. (2008). WASP and SCAR have distinct roles in activating the Arp2/3 complex during myoblast fusion. *J. Cell Sci.* **121**, 1303-1313.

Bour, B. A., Chakravarti, M., West, J. M. and Abmayr, S. M. (2000). *Drosophila* Sns, a member of the Immunoglobulin Superfamily that is essential for myoblast fusion. *Genes Dev.* **14**, 1498-1511.

Chang, H. C., Newmyer, S. L., Hull, M. J., Ebersold, M., Schmid, S. L. and Mellman, I. (2002). Hsc70 is required for endocytosis and clathrin function in Drosophila. *J. Cell Biol.* **159**, 477-487.

Chen, C. M., Freedman, J. A., Bettler, D. R., Jr, Manning, S. D., Giep, S. N., Steiner, J. and Ellis, H. M. (1996). Polychaetoid is required to restrict segregation of sensory organ precursors from proneural clusters in Drosophila. *Mech. Dev.* **57**, 215-227.
Crossley, A. C. (1985). Nephrocytes and pericardial cells. In *Comprehensive Insect Physiology, Biochemistry and Pharmacology*, vol. 3, pp. 487-516. Oxford: Pergamon Press.
Donoviel, D. B., Freed, D. D., Vogel, H., Potter, D. G., Hawkins, E., Barrish, J. P., Mathur, B. N., Turner, C. A., Geske, R., Montgomery, C. A. et al. (2001). Proteinuria and perinatal lethality in mice lacking NEPH1, a novel protein with homology to NEPHRIN. *Mol. Cell. Biol.* **21**, 4829-4836.
Duan, H., Skeath, J. B. and Nguyen, H. T. (2001). Drosophila Lame duck, a novel member of the Gli superfamily, acts as a key regulator of myogenesis by controlling fusion-competent myoblast development. *Development* **128**, 4489-4500.
Dworak, H. A., Charles, M. A., Pellerano, L. B. and Sink, H. (2001). Characterization of Drosophila hibris, a gene related to human nephrin. *Development* **128**, 4265-4276.
Galletta, B. J., Chakravarti, M., Banerjee, R. and Abmayr, S. M. (2004). Sns: adhesive properties, localization requirements and ectodomain dependence in S2 cells and embryonic myoblasts. *Mech. Dev.* **121**, 1455-1468.
Garg, P., Verma, R., Nihalani, D., Johnstone, D. B. and Holzman, L. B. (2007). Neph! cooperates with nephrin to transduce a signal that induces actin polymerization. *Mol. Cell. Biol.* **27**, 8698-8712.
Gerke, P., Huber, T. B., Sellin, L., Benzing, T. and Walz, G. (2003). Homodimerization and heterodimerization of the glomerular podocyte proteins nephrin and NEPH1. *J. Am. Soc. Nephrol.* **14**, 918-926.
Halachmi, N., Feldman, M., Kimchi, Z. and Lev, Z. (1995). Rop and Ras2, members of the Sec1 and Ras families, are localized in the outer membranes of labyrinthine channels and vesicles of Drosophila nephrocyte, the garland cell. *Eur. J. Cell Biol.* **67**, 275-283.
Hamano, Y., Grunkemeyer, J. A., Sudhakar, A., Zeisberg, M., Cosgrove, D., Morello, R., Lee, B., Sugimoto, H. and Kalluri, R. (2002). Determinants of vascular permeability in the kidney glomerulus. *J. Biol. Chem.* **277**, 31154-31162.
Hartenstein, V. (1993). Atlas of *Drosophila* development. In *The Development of Drosophila Melanogaster* (ed. M. Bate and A. Martinez Arias). Cold Spring Harbor, NY: Cold Spring Harbor Laboratory Press.
Holzman, L. B., St John, P. L., Kovari, I. A., Verma, R., Holthofer, H. and Abrahamson, D. R. (1999). Nephrin localizes to the slit pore of the glomerular epithelial cell. *Kidney Int.* **56**, 1481-1491.
Huber, T. B., Schmidts, M., Gerke, P., Schermer, B., Zahn, A., Hartleben, B., Sellin, L., Walz, G. and Benzing, T. (2003). The carboxyl terminus of Neph family members binds to the PDZ domain protein zonula occludens-1. *J. Biol. Chem.* **278**, 13417-13421.
Jones, N., Blasutig, I. M., Eremina, V., Ruston, J. M., Bladt, F., Li, H., Huang, H., Larose, L., Li, S. S., Takano, T. et al. (2006). Nck adaptor proteins link nephrin to the actin cytoskeleton of kidney podocytes. *Nature* **440**, 818-823.
Kestila, M., Lenkkeri, U., Mannikko, M., Lamerdin, J., McCready, P., Putaala, H., Ruotsalainen, V., Morita, T., Nissinen, M., Peltonen, L. et al. (1998). Positionally cloned gene for a novel glomerular protein-Nephrin-is mutated in congenital nephrotic syndrome. *Mol. Cell* **1**, 572-582.
Khoshnoodi, J., Sigmundsson, K., Ofverstedt, L. G., Skoglund, U., Obrink, B., Wartiovaara, J. and Tryggvason, K. (2003). Nephrin promotes cell-cell adhesion through homophilic interactions. *Am. J. Pathol.* **163**, 2337-2346.
Kim, S., Shilagardi, K., Zhang, S., Hong, S. N., Sens, K. L., Bo, J., Gonzalez, G. A. and Chen, E. H. (2007). A critical function for the actin cytoskeleton in targeted exocytosis of prefusion vesicles during myoblast fusion. *Dev. Cell* **12**, 571-586.
Kocherlakota, K. S., Wu, J. M., McDermott, J. and Abmayr, S. M. (2008). Analysis of the cell adhesion molecule sticks-and-stones reveals multiple redundant functional domains, protein-interaction motifs and phosphorylated tyrosines that direct myoblast fusion in Drosophila melanogaster. *Genetics* **178**, 1371-1381.
Koenig, J. H. and Ikeda, K. (1990). Transformational process of the endosomal compartment in nephrocytes of Drosophila melanogaster. *Cell Tissue Res.* **262**, 233-244.
Kosaka, T. and Ikeda, K. (1983). Reversible blockage of membrane retrieval and endocytosis in the garland cell of the temperature-sensitive mutant of Drosophila melanogaster, shibirets1. *J. Cell Biol.* **97**, 499-507.
Liu, G., Kaw, B., Kurfis, J., Rahmanuddin, S., Kanwar, Y. S. and Chugh, S. S. (2003). Neph1 and nephrin interaction in the slit diaphragm is an important determinant of glomerular permeability. *J. Clin. Invest.* **112**, 209-221.
Lu, W., Katz, S., Gupta, R. and Mayer, B. J. (1997). Activation of Pak by membrane localization mediated by an SH3 domain from the adaptor protein Nck. *Curr. Biol.* **7**, 85-94.
Menon, S. D., Osman, Z., Chenchill, K. and Chia, W. (2005). A positive feedback loop between Dumbfounded and Rolling pebbles leads to myotube enlargement in Drosophila. *J. Cell Biol.* **169**, 909-920.
Nagata, M., Yamaguchi, Y., Komatsu, Y. and Ito, K. (1995). Mitosis and the presence of binucleate cells among glomerular podocytes in diseased human kidneys. *Nephron* **70**, 68-71.
Narita, K., Tsuruhara, T., Koenig, J. H. and Ikeda, K. (1989). Membrane pinch-off and reinsertion observed in living cells of Drosophila. *J. Cell. Physiol.* **141**, 383-391.
Patrakka, J. and Tryggvason, K. (2007). Nephrin-a unique structural and signaling protein of the kidney filter. *Trends Mol. Med.* **13**, 396-403.
Putaala, H., Soininen, R., Kilpelainen, P., Wartiovaara, J. and Tryggvason, K. (2001). The murine nephrin gene is specifically expressed in kidney, brain and pancreas: inactivation of the gene leads to massive proteinuria and neonatal death. *Hum. Mol. Genet.* **10**, 1-8.
Richardson, B. E., Beckett, K., Nowak, S. J. and Baylies, M. K. (2007). SCAR/WAVE and Arp2/3 are crucial for cytoskeletal remodeling at the site of myoblast fusion. *Development* **134**, 4357-4367.
Rohatgi, R., Nollau, P., Ho, H. Y., Kirschner, M. W. and Mayer, B. J. (2001). Nck and phosphatidylinositol 4,5-bisphosphate synergistically activate actin polymerization through the N-WASP-Arp2/3 pathway. *J. Biol. Chem.* **276**, 26448-26452.
Ruiz-Gomez, M., Coutts, N., Price, A., Taylor, M. V. and Bate, M. (2000). *Drosophila* Dumbfounded: a myoblast attractant essential for fusion. *Cell* **102**, 189-198.
Ruotsalainen, V., Ljungberg, P., Wartiovaara, J., Lenkkeri, U., Kestila, M., Jalanko, H., Holmberg, C. and Tryggvason, K. (1999). Nephrin is specifically located at the slit diaphragm of glomerular podocytes. *Proc. Natl. Acad. Sci. USA* **96**, 7962-7967.
Ruotsalainen, V., Patrakka, J., Tissari, P., Reponen, P., Hess, M., Kestila, M., Holmberg, C., Salonen, R., Heikinheimo, M., Wartiovaara, J. et al. (2000). Role of nephrin in cell junction formation in human nephrogenesis. *Am. J. Pathol.* **157**, 1905-1916.
Rusten, T. E., Rodahl, L. M., Pattni, K., Englund, C., Samakovlis, C., Dove, S., Brech, A. and Stenmark, H. (2006). Fab1 phosphatidylinositol 3-phosphate 5-kinase controls trafficking but not silencing of endocytosed receptors. *Mol. Biol. Cell* **17**, 3989-4001.
Sellin, L., Huber, T. B., Gerke, P., Quack, I., Pavenstadt, H. and Walz, G. (2003). NEPH1 defines a novel family of podocin interacting proteins. *FASEB J.* **17**, 115-117.
Shelton, C., Kocherlakota, K. S., Zhuang, S. and Abmayr, S. M. (2009). The immunoglobulin superfamily member Hbs functions redundantly with Sns in interactions between founder and fusion-competent myoblasts. *Development* **136**, 1159-1168.
Strunkelnberg, M., Bonengel, B., Moda, L. M., Hertenstein, A., de Couet, H. G., Ramos, R. G. and Fischbach, K. F. (2001). rst and its paralogue kirre act redundantly during embryonic muscle development in Drosophila. *Development* **128**, 4229-4239.
Takahisa, M., Togashi, S., Suzuki, T., Kobayashi, M., Murayama, A., Kondo, K., Miyake, T. and Ueda, R. (1996). The Drosophila tamou gene, a component of the activating pathway of extramacrochaetae expression, encodes a protein homologous to mammalian cell-cell junction-associated protein ZO-1. *Genes Dev.* **10**, 1783-1795.
Tepass, U. (1996). Crumbs, a component of the apical membrane, is required for zonula adherens formation in primary epithelia of Drosophila. *Dev. Biol.* **177**, 217-225.
Tryggvason, K. (1999). Unraveling the mechanisms of glomerular ultrafiltration: nephrin, a key component of the slit diaphragm. *J. Am. Soc. Nephrol.* **10**, 2440-2445.
Tryggvason, K., Ruotsalainen, V. and Wartiovaara, J. (1999). Discovery of the congenital nephrotic syndrome gene discloses the structure of the mysterious molecular sieve of the kidney. *Int. J. Dev. Biol.* **43**, 445-451.
Verma, R., Kovari, I., Soofi, A., Nihalani, D., Patrie, K. and Holzman, L. B. (2006). Nephrin ectodomain engagement results in Src kinase activation, nephrin phosphorylation, Nck recruitment, and actin polymerization. *J. Clin. Invest.* **116**, 1346-1359.
Wartiovaara, J., Ofverstedt, L. G., Khoshnoodi, J., Zhang, J., Makela, E., Sandin, S., Ruotsalainen, V., Cheng, R. H., Jalanko, H., Skoglund, U. et al. (2004). Nephrin strands contribute to a porous slit diaphragm scaffold as revealed by electron tomography. *J. Clin. Invest.* **114**, 1475-1483.
Weavers, H., Prieto-Sanchez, S., Grawe, F., Garcia-Lopez, A., Artero, R., Wilsch-Brauninger, M., Ruiz-Gomez, M., Skaer, H. and Denholm, B. (2009). The insect nephrocyte is a podocyte-like cell with a filtration slit diaphragm. *Nature* **457**, 322-326.
Wigglesworth, V. B. (1972). *The Principles of Insect Physiology*, 7th edn., pp. 440-442. New York: Chapman & Hall.

Table S1. TUNEL analysis for third instar Garland cells

Genotype	Imaged nuclei (sample)	TUNEL positive	
		Number of positive signals	%
sns-GCN-nGFP, sns-GCN-Gal4/+	181 (4)	6	3.31
sns-GCN-nGFP, sns-GCN-Gal4/UAS-sns-IR(1)	180 (4)	70	38.90
sns-GCN-nGFP, sns-GCN-Gal4/UAS-sns-IR(2)	93 (4)	38	40.86
sns-GCN-nGFP, sns-GCN-Gal4/UAS-duf-IR(1)	102 (3)	52	50.90
sns-GCN-nGFP, sns-GCN-Gal4/UAS-duf-IR(2)	109 (4)	18	16.51
$sns^{4.3}$, Act5C-Gal4/$sns^{4.3}$, UAS-2xEGFP	83 (4)	36	43.37
sns-GCN-nGFP, sns-GCN-Gal4/UAS-pyd-IR	144 (4)	14	9.72
sns-Gal4/$sns^{zf1.4}$, UAS-sns[C-HA]	66 (3)	0	0
$sns^{zf1.4}$, sns-Gal4/$sns^{zf1.4}$, UAS-sns[C-HA]	101 (4)	22	21.80
sns-Gal4/$sns^{zf1.4}$, UAS-sns[mIg4]	64 (4)	18	28.13
$sns^{zf1.4}$, sns-Gal4/$sns^{zf1.4}$, UAS-sns[mIg4]	34 (3)	16	47.06
sns-Gal4/$sns^{zf1.4}$, UAS-sns[mIg6]	92 (3)	0	0
$sns^{zf1.4}$, sns-Gal4/$sns^{zf1.4}$, UAS-sns[mIg6]	25 (3)	17	68.00